AGU PUBLICATIONS

Geophysical Research Letters

RESEARCH LETTER
10.1002/2015GL063868

Key Points:
- Intense turbulence associated with vertical moisture gradients up to 5 km
- Uncertain resultant mixing by intermittent turbulence: three methods compared
- Potential role in moisture budget during subsident period or after dry intrusion

Correspondence to:
H. Bellenger,
hbellenger@jamstec.go.jp

Citation:
Bellenger, H., M. Katsumata, and K. Yoneyama (2015), Turbulent mixing and its impact on lower tropospheric moisture over tropical ocean, *Geophys. Res. Lett.*, *42*, doi:10.1002/2015GL063868.

Received 16 MAR 2015
Accepted 26 MAR 2015
Accepted article online 27 MAR 2015

Turbulent mixing and its impact on lower tropospheric moisture over tropical ocean

Hugo Bellenger[1], Masaki Katsumata[1], and Kunio Yoneyama[1]

[1]Japan Agency for Marine-Earth Science and Technology, Yokosuka, Japan

Abstract The variability of lower tropospheric humidity is a crucial feature of the tropical climate. Among the processes that impact moisture budget, the vertical transport by turbulent mixing is generally overlooked. Using observations from Cooperative Indian Ocean experiment on intraseasonal variability/Dynamics of the Madden-Julian Oscillation (MJO), CINDY/DYNAMO, campaign, this is a first attempt to quantify it over the tropical ocean. Turbulent patches of ~100 m depth are observed in relation with large vertical gradients of specific humidity. Intense mixing is diagnosed within these intermittent patches. Three approaches are used to diagnose the overall effect of this intermittent turbulence. Large uncertainties on the corresponding eddy diffusivity coefficient arise from parameters hard to experimentally constrain. However, dry conditions are associated with steep moisture vertical gradients above the boundary layers. Owing to the uncertainties on the eddy diffusivity, these gradients can correspond to negligible or to significant moisture tendencies (~0.5–1 g kg^{-1} d^{-1}) during the recovery following a dry intrusion or the preconditioning stage of an MJO.

1. Introduction

Over tropical oceans, moist convection is sensitive to the lower (~1–4 km height) tropospheric water vapor content [*Holloway and Neelin*, 2009]. This sensitivity plays certainly a role in shaping the tropical variability from local-scale to large-scale phenomena such as the Madden-Julian Oscillation (MJO) [*Benedict and Randall*, 2007]. Yet moisture shows a great variability over tropical oceans due to diverse phenomena spanning from large-scale subsidence to sudden and more localized dry intrusions [*Redelsperger et al.*, 2002]. In addition, fine-scale structures such as layers of a few hundreds of meters depth are visible in the lower free troposphere over tropical oceans [*Davison et al.*, 2013a, 2013b]. A major issue in understanding and simulating the tropospheric moisture budget is that local moisture tendencies are usually comparable to any of the budget term: large-scale horizontal and vertical advections but also convective processes [*Bellenger et al.*, 2015]. The role of turbulent mixing in the lower troposphere moisture budget is generally overlooked. Still, steep vertical gradients of moisture above the boundary layer are observed during suppressed phase of MJO [*Yoneyama et al.*, 2013] or following dry intrusions [*Redelsperger et al.*, 2002]. These gradients are likely to be impacted by the diffusive-like vertical transport induced by turbulent mixing.

Clear air turbulence (CAT) is a process that impacts the atmosphere dynamics, energetics, chemical species distribution, and aviation [*Williams and Joshi*, 2013]. In the free atmosphere, CAT occurs intermittently within horizontally extending patches. This makes difficult to quantify its resulting mixing [*Vanneste and Haynes*, 2000] although it is usually characterized by a vertical eddy diffusivity coefficient. The sources of CAT are diverse (instabilities due to wind shear, gravity and inertia-gravity waves breaking, and convection) with diverse spatiotemporal scales. Yet CAT is still poorly documented, and past observational studies mainly concentrated on upper troposphere and stratosphere over continental area with the notable exception of *Alappattu and Kunhikrishnan* [2010]. The eddy diffusivities that were diagnosed in the free troposphere spanned over a wide range from 10^{-2} to 10^{2} m^2 s^{-1} [e.g., *Wilson*, 2004]. This study is a first attempt to diagnose the CAT turbulent eddy diffusivity and its impact on moisture turbulent vertical transport in the lower troposphere over the tropical open ocean.

2. Data and Method

We use observations from the R/V *Mirai* during the Cooperative Indian Ocean experiment on intraseasonal variability/Dynamics of the MJO (CINDY/DYNAMO) campaign [*Yoneyama et al.*, 2013]. The R/V *Mirai* was then situated in the central Indian Ocean (80.5°E–8°S); it mainly monitored shallow convective situations

[*Bellenger et al.*, 2015] and experienced dry air intrusions [*Kerns and Chen*, 2014]. We use 376 atmospheric profiles from 3-hourly launches of Vaisala RS92-SGPD sondes from the Special Observing Period (SOP, 7 October 2011 to 28 November 2011 [*Ciesielski et al.*, 2014]). Data are recorded every 2 s which corresponds to an average vertical resolution of ~7 m. We thus interpolate the soundings data with a regular step of 7 m. From these soundings, we intend to quantify the eddy diffusivity and its impact on moisture tendencies and reveal the associated uncertainties. Three methods are applied to determine the eddy diffusivity coefficient: two are based on Thorpe method [*Thorpe*, 1977] and one on mixing length theory [*Hong and Pan*, 1996] as detailed below. To contrast dry and moist conditions, we use the anomaly of the mean specific humidity between 2 and 4 km where the maximum specific humidity variations are found and because convection is particularly sensitive to the moisture in this layer [*Holloway and Neelin*, 2009]. Soundings with negative/positive anomalies of less/more than a certain threshold are classified as dry/moist condition. There are 132 soundings in each category by defining this threshold as half the standard deviation for the entire SOP.

3. Eddy Diffusivity Computations

3.1. Mixing Length Theory

We first use a diagnostic of eddy diffusivity coefficient based on the mixing length formulation of *Hong and Pan* [1996] and typical of Richardson number-based parameterization. As in *Clayson and Kantha* [2008] we do not consider any background diffusion (set to 1 $m^2 s^{-1}$ by *Hong and Pan* [1996]). It reads $K_{Ri} = l^2 |\partial U/\partial z| f(Ri_g)$ where U is the horizontal wind speed, f is a stability function depending on the stratification of the atmosphere and thus on the sign of the gradient Richardson number Ri_g, l is the mixing length with $1/l = (1/\kappa z) + (1/l_0)$, κ is the von Karman constant, and $l_0 = 30$ m.

3.2. Thorpe Analysis

The Thorpe analysis [*Thorpe*, 1977] has been originally designed to characterize overturns produced by turbulence in the water by comparing the observed potential density profile with the corresponding stable (monotonic) profile constructed by reordering the water parcels. The displacements of the parcels define the Thorpe length scale L_T that is a proxy for the Ozmidov scale L_O [*Ozmidov*, 1965]. L_O is a function of the turbulent kinetic energy dissipation rate and of the Brunt-Vaisala frequency and represents the upper limit of eddy size under a given stratification. It corresponds to the scale for which inertia and buoyancy forces are in equilibrium and is linked to eddy diffusivity [e.g., *Gavrilov et al.*, 2005]. The Thorpe analysis has been recently applied to the atmosphere by using soundings potential temperature (θ) profiles [*Gavrilov et al.*, 2005; *Clayson and Kantha*, 2008; *Wilson et al.*, 2010, hereafter W10]. By comparing Thorpe analysis and radar measurements, *Luce et al.* [2014] showed that it indeed catches active turbulence in the atmosphere. W10 proposes in addition an objective approach to reject spurious overturns created by instrumental noise. We only give a short presentation of this method as it is fully described in W10.

The instrumental noise variance σ_N is diagnosed as the half of the variance of the detrended data on 200 m segments for the entire data set (W10). It is first used to determine the optimal vertical resolution to be used for the Thorpe analysis. In our case, a denoising procedure is necessary and a three-step smoothing and an undersampling of factor 3 are used, reducing our vertical resolution to a 21 m resolution data set. Then, we sort the potential temperature profile and determine the Thorpe displacements defined as $D(i) = (i - R(i))\,dz$ where $R(i)$ is the rank of the ith bin in the reordered profile and $dz = 21$ m. Then an inversion is defined as a region where $\sum_{i=1,n} D(i) = 0$ and $\sum_{i=1,k} D(i) < 0$ for any $k < n$ to ensure that displacements are negative (positive) at the bottom (top) of an inversion (W10). Finally, the actual overturns are identified from inversions by imposing that the range of θ variation within the inversion exceeds the 99% of the noise range for a sample of equivalent size and a standard deviation equal to σ_N. W10 provides the tabulated percentiles of the range for normally distributed random variables as a function of the sample size. For each overturn, the Thorpe length scale L_T is simply computed as the RMS of the Thorpe displacements. Within each overturn, the eddy diffusivity can be computed as $K_{Th} = \gamma C_K L_T^2 N$ [*Gavrilov et al.*, 2005; *Clayson and Kantha*, 2008] where N is the Brunt-Vaisala frequency that is computed on the reorganized stable profile of θ [*Wilson et al.*, 2014] and with the mixing efficiency taken as $\gamma = 0.25$. Outside the selected overturns, the eddy diffusivity is zero. The value of C_K is largely uncertain and typically ranges between 6.10^{-2} and 16 [*Clayson*

and Kantha, 2008]. Following *Kantha and Hocking* [2011], we take $C_K = 1$, as they found that it gives the best agreement with radar-derived estimates. However, one should keep in mind that as the eddy diffusivity coefficient is proportional to C_K, its diagnostic is affected by this large uncertainty.

One should note that static stability is decreased in saturated air due to the latent heat release by water condensation. *Wilson et al*. [2013] proposed an approach to take this effect into account that strongly increase the diagnosed turbulent fraction of the troposphere. However, in our case, saturated air mostly corresponds to moist convection for which the formulations of turbulence parameters in stratified environment are not adapted [*Wilson et al*., 2014]. We then use the simplified approach of *Wilson et al*. [2013] based on *Zhang et al*. [2010] to remove cloudy and mostly convective sections of the profiles before performing the Thorpe analysis on θ. We thus focus on CAT when the atmosphere is statically stable. In addition, in the free atmosphere, turbulence is a highly intermittent phenomenon: CAT patches correspond to highly localized and intense moisture fluxes and tendencies. Therefore, the mean $\overline{K_{\mathrm{Th}}}(z)$ of the eddy diffusion coefficients $K_{\mathrm{Th}}(z)$ (only defined within overturns) may not represent the actual effective eddy diffusion coefficient by intermittent turbulence patches occurrences [*Dewan*, 1981; *Woodman and Rastogi*, 1984; *Vanneste and Haynes*, 2000; *Wilson*, 2004]. We thus also consider the effective eddy diffusivity coefficient proposed by *Vanneste and Haynes* [2000]. This coefficient is computed as $K_{\mathrm{eff}} = F_T\overline{d^3}/\left(12\overline{d}\tau_L\right)$ where F_T is the turbulent air fraction with respect to clear air, d is the overturns thickness, and τ_L is the mean lifetime of a turbulent patch. Turbulence characteristics are based on all overturns occurring between 1 and 5 km to avoid taking into account turbulence from the turbulent boundary layer. The overbars indicate an averaging over all soundings. The sensitivity of the eddy diffusivities computation over selected periods (dry and moist conditions) will be discussed below.

The three diagnostics of the eddy diffusivity are based on several assumptions and parameters that are difficult to constrain from observation ($f(Ri_g)$, C_K, F_T, d, and τ_L). We discuss in this study the induced uncertainties on turbulent mixing and on its role in moisture variations. The vertical resolution of our observations limits our detection to the larger overturns ($\geq$42 m). These overturns represent a small number of the total overturns [*Wilson et al*., 2011]. We might thus underestimate the actual turbulent fraction F_T of the lower troposphere. But on the other hand, we also overestimate the statistics of overturn's thickness d. The potential impact of this limitation on our results for K_{eff} is discussed below. Another issue is the evaluation of the patches lifetime τ_L distribution that is largely unknown. Observations by *Wilson et al*. [2005, Figures 1a and 2a] suggest that turbulent patches with ~100 m depth have a lifetime of ~1 h. So we set $\tau_L = 1$ h and will discuss the sensitivity of our results to this choice.

Finally, we compute the turbulent fluxes and moisture tendencies based on the mean profile of eddy diffusivity computed from mixing length theory, Thorpe analysis (smoothed over 1 km), and from the effective diffusivity coefficient following $\overline{\omega' q'} = -K(\partial q/\partial z)$, with $K = \overline{K_{Ri}}$, $\overline{K_{\mathrm{Th}}}$, and K_{eff}, and $\partial q/\partial t|_{\mathrm{Turb.}} = -\partial\overline{\omega' q'}/\partial z$. The vertical derivatives are computed by linear regression over an interval of 1 km to get reasonable amount of points and smooth results. The main features discussed here are not sensitive to this choice. For depiction of fine structures in the vertical distribution of moisture, the vertical variations of the specific humidity shown in Figure 1 are, however, computed on 200 m intervals.

4. Results

Figure 1 shows the vertical gradient profiles of specific humidity observed by radiosondes launched at R/V *Mirai* during CINDY/DYNAMO in clear air (clouds are shaded in white). Large variations in the vertical gradients of specific humidity are evident mainly up to 5 km on the scale of a few hundreds of meters. These variations are indicative of a layered structure of moisture in the lower troposphere that has been revealed using Bragg scattering from *S* band radar by *Davison et al*. [2013a, 2013b] over Barbuda during Rain in Cumulus over the Ocean experiment and over Gan Island during CINDY/DYNAMO [*Davison*, 2014]. Figure 1 also shows the turbulent layers diagnosed from Thorpe analysis (black segments) and the SOP mean turbulent air fraction F_T profile. First, the turbulent boundary layer is evident between surface and roughly 500 m height. There, F_T reaches 50%. Above, the turbulent patches are intermittent with F_T of less than 10% and a secondary maximum around 3–4 km. Note that these values of F_T are slightly weaker than those reported by *Wilson et al*. [2005] in the upper troposphere using radar techniques. Interestingly, most

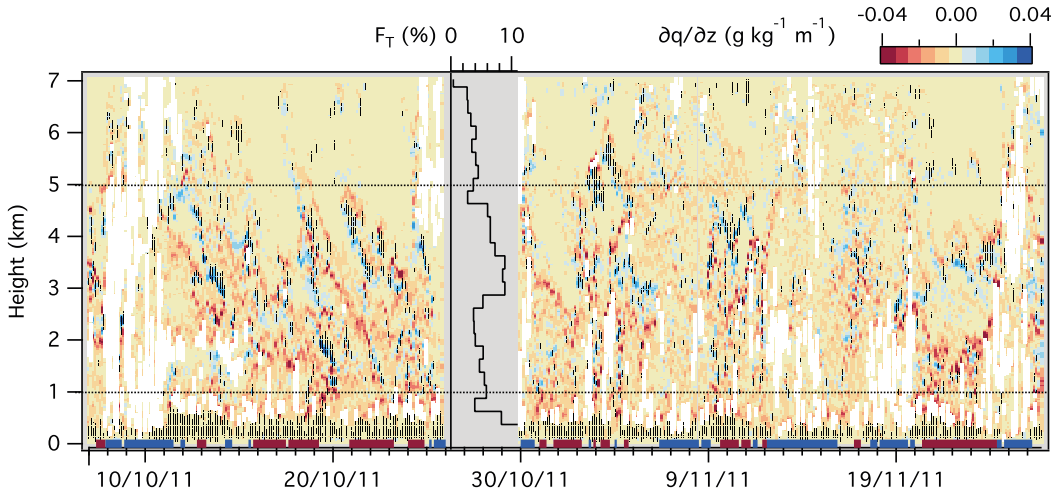

Figure 1. Vertical gradient of specific humidity (colors, g kg^{-1} m^{-1}) during CINDY campaign SOP. Black segments denote turbulent layers diagnosed by the Thorpe analysis, white shading indicates cloudy area, and the black distribution (top axis) gives the mean profile of the clear air turbulent fraction F_T (%) for the SOP. Red/blue ticks on the bottom axis denote time steps defined as dry/moist conditions. The grey shading represents the period between the two legs when R/V *Mirai* was not at its position.

turbulent patches diagnosed here correspond to relatively weak wind conditions with the largest patches being usually associated with vertical shear (not shown). These turbulent patches are also associated with large vertical humidity gradients. Conversely, there are very few turbulent patches where this vertical gradient is close to zero around 5 km and above. However, not all the strong moisture gradients are

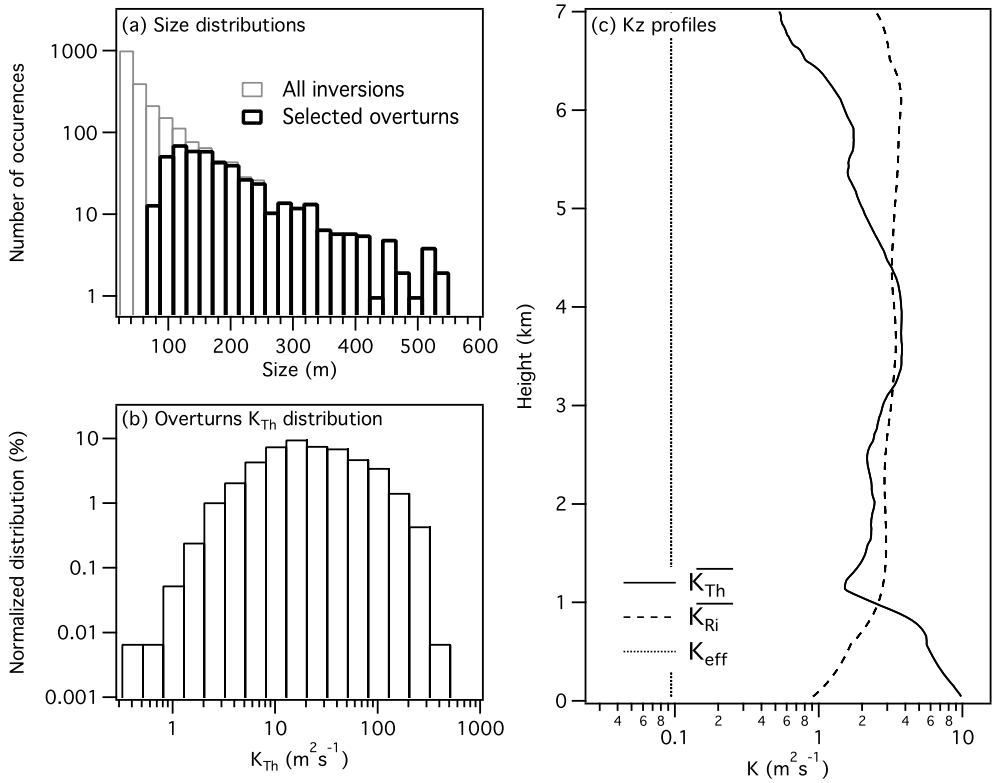

Figure 2. Distributions of (a) the size of all the detected inversions (grey) and of the remaining overturns after applying the selection procedure (black) between 1 and 5 km and (b) the eddy diffusivity coefficient K_{Th} in the selected overturns between 1 and 5 km; (c) the vertical profiles of mean turbulent diffusivities $\overline{K_{Th}}$ from Thorpe analysis (solid), $\overline{K_{Ri}}$ from mixing length theory, and the effective eddy diffusivity K_{eff} following *Vanneste and Haynes* [2000] (dotted vertical line).

associated with turbulent patches (e.g., on 21 October at 2 km). *Davison et al*. [2013b] present some statistics of the lifetime over the radar of Bragg scattering layers associated with moisture vertical gradients. They found a median lifetime of about 8 h with 25% having a lifetime of more than 20 h. Here some turbulent patches, usually the largest, seem to be continuously monitored over several successive soundings (e.g., 14 October at 3 km, 20 October at 2 km, and 10 November at 4 km) corresponding to timescales of up to 20 h. Yet most turbulent patches appear isolated in time in Figure 1 and may thus correspond to smaller spatiotemporal scales. The moist layers are thought to be produce by turbulent mixing or cloud detrainment that certainly also involves turbulence [*Davison et al*., 2013a]. The discrepancy in their apparent lifetimes thus suggests that the moisture layers have a longer lifetime than the process that generates them. Finally, the sources of CAT may not be here exactly the same nor have the same characteristics as *Davison et al*. [2013a, 2013b]; *Davison* [2014] report observations over islands and not open ocean.

Figure 2 provides further statistics on lower free troposphere turbulence observed by R/V *Mirai* at 1–5 km where most of CAT is observed (Figure 1). In Figure 2a, the size distribution of all inversions detected (about 2300) is plotted together with the size distribution of the actual overturns selected with a confidence of 99% (about 490, W10). The selection method mainly removes smaller inversions as being due to instrumental noise. The selected overturns have a minimum size of ~80 m and the distribution peaks at ~120 m. The larger patches have a size of ~500 m. The distribution of K_{Th} within these overturns is plotted in Figure 2b. It shows a great variability spanning over 3 orders of magnitude (1–100 $\mathrm{m^2\,s^{-1}}$) with a peak of the distribution around 10–20 $\mathrm{m^2\,s^{-1}}$. This is comparable to the values reported by *Wilson et al*. [2014]. Figure 2c presents the mean eddy diffusivity coefficients profile over the whole R/V *Mirai* observation period as deduced from Thorpe analysis $\overline{K_{\mathrm{Th}}}$ (solid) and mixing length theory $\overline{K_{Ri}}$ (dashed). The effective eddy diffusivity coefficient K_{eff} [*Vanneste and Haynes*, 2000] is also plotted (vertical dotted line). Between 1.5 km and 4.5 km heights, $\overline{K_{\mathrm{Th}}}$ and $\overline{K_{Ri}}$ are in good agreement with each other (about 1–2 $\mathrm{m^2\,s^{-1}}$) and fall within the large range of previously reported values [*Wilson*, 2004, Table 1]. Using 44 soundings over the northern Indian Ocean, *Alappattu and Kunhikrishnan* [2010] reported smaller values of eddy diffusivity of about 0.1–1 $\mathrm{m^2\,s^{-1}}$. This discrepancy may be largely explained by their taking $C_K = 0.3$ ($C_K = 1$ here). The effective eddy diffusivity coefficient is found to be an order of magnitude smaller than $\overline{K_{\mathrm{Th}}}$ and $\overline{K_{Ri}}$ ($K_{\mathrm{eff}} \sim 0.1\ \mathrm{m^2\,s^{-1}}$). The vertical resolution of our measurements certainly impacts our diagnostic of turbulent patches. On one hand, we underestimate the turbulent air fraction F_T by omitting the smallest patches. On the other hand, we overestimate the layer size statistics by omitting these small patches and artificially creating large patches by merging several neighboring patches. A way to test the sensitivity of K_{eff} is to compute the effective eddy diffusivity based on all detected inversions rather than over selected overturns only. The effective eddy diffusivity K_{eff} then rises only by 5%. Thus, the two antagonist effects seem to largely cancel out. However, K_{eff} also strongly depends on the turbulence lifetime τ_L that is largely unknown and certainly depend on the spatial scale of the turbulent patch. Here an average lifetime of 5 min would make $K_{\mathrm{eff}} \approx 1\ \mathrm{m^2\,s^{-1}}$ and comparable to the two other estimates.

In order to highlight the impact of CAT on moisture budget, we contrast the SOP driest conditions from the most humid ones. The specific humidity profiles for these two categories are presented in Figure 3a together with their corresponding mean profiles. The time periods corresponding to these conditions are is reported in Figure 1 (bottom axis). The moist conditions correspond to more clouds (Figure 1). However, the turbulent air fraction relative to clear air is about twice as large for dry conditions (8% on the average between 1 and 5 km and reaching 12% around 4 km) than for moist conditions (4% between 1 and 5 km). Furthermore, larger turbulent patches are observed during dry conditions (not shown). Then, between 1 and 5 km, eddy diffusivity coefficients are larger for dry conditions ($\overline{K_{\mathrm{Th}}} = 3.4\ \mathrm{m^2\,s^{-1}}$ and $K_{\mathrm{eff}} = 0.12\ \mathrm{m^2\,s^{-1}}$) than for moist conditions ($\overline{K_{\mathrm{Th}}} = 1\ \mathrm{m^2\,s^{-1}}$ and $K_{\mathrm{eff}} = 0.05\ \mathrm{m^2\,s^{-1}}$). Another striking difference between the two categories is the strong mean vertical gradient in specific humidity (~5 $\mathrm{g\,kg^{-1}\,km^{-1}}$, Figure 3a) from the top of the boundary layer up to 3 km for dry conditions corresponding to abrupt decreases in moisture for each sounding (Figure 3a). Figure 3b represents the evaluation of moisture tendencies due to turbulent vertical transport diagnosed using the three different eddy diffusivities (Figure 2c). The large tendencies diagnosed using $\overline{K_{\mathrm{Th}}}$ (solid lines) below 1.5 km are associated to the large and sudden decrease in turbulence above the boundary layer (Figure 2c). Above this height, both mean $\overline{K_{\mathrm{Th}}}$ and mean $\overline{K_{Ri}}$ show comparable results. For dry conditions, large positive moisture tendencies of ~0.5–1 $\mathrm{g\,kg^{-1}\,d^{-1}}$ are diagnosed around 2–3 km at the

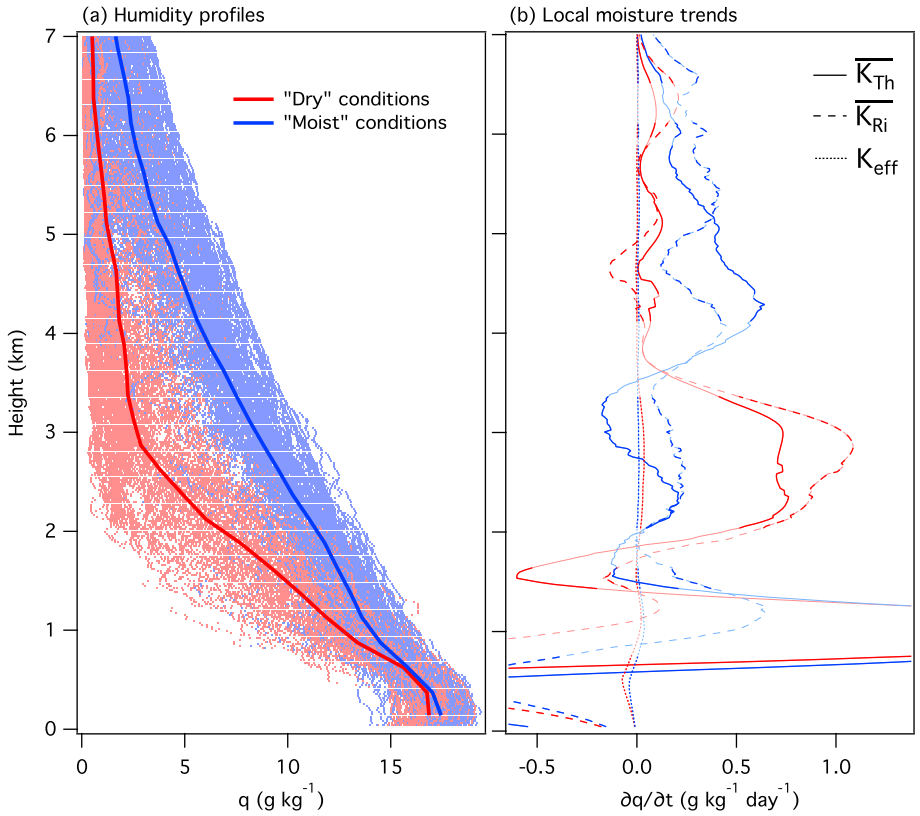

Figure 3. Vertical profiles for dry (red) and moist (blue) conditions of (a) specific humidity (points, g kg^{-1}) and the corresponding average profiles (thick lines) and (b) local moisture tendencies (g kg^{-1} d^{-1}) computed using $\overline{K_{Th}}$ (solid), $\overline{K_{Ri}}$ (dashed), and K_{eff} (dotted). Dark (light) colors indicate that the difference between dry and moist condition trends is (is not) statistically significant to the 99% level using a Student's *t* test. Within the boundary layer, below 500 m, the trends reach −3 and −1.5 g kg^{-1} d^{-1} for dry and moist conditions, respectively, and both reach 3 g kg^{-1} d^{-1} at 1 km height.

top of mean moisture gradient due to vertical convergence of the turbulent moisture flux. The amplitude of this tendency depends on the definition of dry conditions: its order of magnitude remains unchanged, but it tends to increase when only the driest conditions are retained (not shown). Dry intrusions typically create very steep moisture vertical gradient [e.g., *Parsons et al.*, 2000] as the one we can observe on 21 November: a decrease of −10 g kg^{-1} within 500 m at 2–3 km. Following a dry intrusion, the lower troposphere typically takes some days to recover and the moisture to get back to its previous value [e.g., *Redelsperger et al.*, 2002]. Then, these results suggest that turbulent transport may be a nonnegligible process during the recovery phase following a dry intrusion. For moist conditions, there is some turbulent-induced positive moisture tendency at 4–5 km associated with some vertical gradient of moisture there. In comparison, tendencies obtained using K_{eff} (with $\tau_L = 1$ h) are roughly 10 times smaller than the ones obtained with $\overline{K_{Th}}$. There is thus a large uncertainty on the actual importance of turbulent transport for local moisture variations.

5. Summary and Discussion

This study provides diagnostics of turbulent patches in the free troposphere over tropical ocean and a first attempt to quantify from observations the turbulent mixing, its impact on moisture, and the associated uncertainties. CAT can be detected mainly up to 5 km height in association with steep moisture gradients on the scale of a few hundred meters. These gradients are certainly linked with the moisture layers observed by *Davison et al.* [2013a, 2013b] and *Davison* [2014] over the islands of Barbuda and Gan. Part of these layers is certainly created by turbulent patches. Conversely, this could also be indicative of the fact that preferred regions of turbulent patches creation are also regions of large moisture gradients. *Davison et al.* [2013b] suggested that moist layers could arise from cloud detrainment. As convective processes also produce turbulence in neighboring clear air [*Luce et al.*, 2010] turbulence and moisture layers could then

both originate from cloud detrainment. In the case of a dry intrusion, for example, the steep vertical moisture gradient would limit the convective cloud vertical extend and thus select a preferred height for the production of turbulence. The association between turbulent patches and moisture gradients is, however, not systematic. Furthermore, the latter are more persistent than the former. Thus, the typical lifetime of a few hours of these moisture layers [*Davison et al*., 2013b] is certainly an upper boundary for turbulent patches lifetime. Of course, this holds as far as we can compare moisture layers observed here and observed over small islands.

In the lower troposphere above open ocean, intermittent ($F_T \leq 10\%$) turbulent patches with vertical scale of ~100 m correspond to intense mixing (K_{Th} of 1–100 $\mathrm{m^2\,s^{-1}}$). Yet an important result is the large uncertainty on the order of magnitude of the resulting effective eddy diffusivity. Three different estimates of this mean resulting eddy diffusivity are computed: K_{eff}, $\overline{K_{Ri}}$, and $\overline{K_{\mathrm{Th}}}$. All have their uncertainties and sensitivity to parameters that are difficult to estimate from observations (C_K, F_T, and the turbulent patch size d and lifetime τ_L distributions). Here above the turbulent boundary layer, $\overline{K_{Ri}}$ and $\overline{K_{\mathrm{Th}}}$ show good agreement, whereas K_{eff} is 10 times weaker. Still, this uncertainty can be explained by the uncertainty on the parameters on which the eddy diffusivity diagnostics are based. Indeed, $\overline{K_{\mathrm{Th}}} \approx K_{\mathrm{eff}}$ for $C_K = 0.1$ that lies within the uncertainty range for this parameter. Furthermore, due to our observation limitation, we certainly underestimate the fraction of turbulent air F_T; on the other hand, we may overestimate the turbulent patch sizes. A rough sensitivity test shows that these two shortcomings may, however, compensate each other for *Vanneste and Haynes* [2000] K_{eff} formulation. However, *Wilson et al*. [2005] show that CAT consists of numerous short-lived patches (few minutes) that could enhance K_{eff} to 1 $\mathrm{m^2\,s^{-1}}$ if τ_L is taken as 5 min rather than 1 h. Finally, we evaluate F_T for the entire campaign and did not take into account any spatiotemporal inhomogeneity of the turbulent patches distribution. Indeed, CAT seems to be more active during dry conditions and also to preferentially occur in association with strong moisture gradients which could locally enhance the effect of mixing on moisture tendencies.

We finally address the potential impact of CAT on moisture transport in the lower troposphere. It may be negligible in the absence of strong vertical gradient of moisture. Therefore, we separate "moist" and "dry" conditions in our analysis. The latter conditions include periods following dry intrusion when steep vertical gradients in specific humidity, with vertical scales comparable to the one of CAT patches, are typically observed. According to $\overline{K_{Ri}}$ and $\overline{K_{\mathrm{Th}}}$ values, large CAT-induced moisture tendencies of 0.5–1 $\mathrm{g\,kg^{-1}\,d^{-1}}$ are diagnosed at the top of the average vertical gradient of moisture (2–3 km, Figure 3). These tendencies can be compared to average moisture tendencies associated with shallow convection and large-scale advections during the same period (0.5–4 $\mathrm{g\,kg^{-1}\,d^{-1}}$) [*Bellenger et al*., 2015, Figures 7 and 10]. There is thus a possibility that CAT may have a significant impact on steep vertical gradients associated with dry conditions such as these prevailing during the preconditioning stage of an MJO or just following a dry intrusion. On the other hand, according to the present evaluation of K_{eff}, the CAT-induced moisture tendencies are negligible and then potentially overestimated in models (K_{Ri}). We show that we cannot give a definitive conclusion on this issue as it is strongly dependent on parameters that are difficult to observe (e.g. τ_L) and may not be homogeneous in time and space. Indeed, CAT potentially arise in preferred regions associated with moisture gradients. For instance, in the case of the limitation of the convective cloud height at a given altitude by subsidence or dry intrusion-induced steep decrease in moisture, large turbulent patches could also be preferentially produced there in direct association with moisture gradient. This would increase the eddy diffusivity precisely where the turbulent mixing should have the strongest impact on the moisture budget. Then convective processes and turbulent mixing may act together to moisten up the troposphere.

There are only few studies trying to quantify CAT characteristics in the tropical lower troposphere in open ocean region, and this is the first to attempt quantifying its impact on vertical moisture transport. In this context, turbulent mixing is generally overlooked. However, it is largely unknown and might not be negligible. The large uncertainties on the turbulent transport of moisture certainly deserve further attention in order to be correctly taken into account in models. Thus, additional diagnostics, using regular soundings or high-resolution soundings [*Balsley et al*., 2010; *Marlton et al*., 2015] and radars, are necessary to better constrain observable CAT parameters. In particular, diagnosing the turbulent patch size and lifetime distributions is of prime importance to reduce the uncertainties on the strength of turbulent

transport of water vapor or any chemical specie. We did not include the effect of moisture on the turbulence detection [*Wilson et al*., 2013] in order to avoid treating convection as turbulence. This impact has also to be addressed to evaluate the effect of turbulence near clouds. Finally, the origin of the turbulent patches was let out of the scope of the present article and is let for future studies.

Acknowledgments
The authors would like to thank Captain Y. Ishioka, his crew, and technical staff of Global Ocean Development Inc. for their support of observations on board R/V *Mirai*. The authors also would like to thank R. Wilson and F. Dalaudier for their useful conversations on the present study. The Editor and two anonymous reviewers are acknowledged for their constructive comments on this manuscript. The data used in this study are available online: http://www.jamstec.go.jp/iorgc/cindy/obs/obs.html.

The Editor thanks two anonymous reviewers for their assistance in evaluating this paper.

References

Alappattu, D. P., and P. K. Kunhikrishnan (2010), First observations of turbulence parameters in the troposphere over the Bay of Bengal and the Arabian Sea using radiosonde, *J. Geophys. Res.*, *115*, D06105, doi:10.1029/2009JD012916.

Balsley, B. B., L. Kantha, and W. Colgan (2010), On the use of Slow Ascent Meter-Scale Sampling (SAMS) radiosondes for observing overturning events in the free atmosphere, *J. Atmos. Oceanic Technol.*, *27*, 766–775.

Bellenger, H., K. Yoneyama, M. Katsumata, T. Nishizawa, K. Yasunaga, and R. Shirooka (2015), Observation of moisture tendencies related to shallow convection, *J. Atmos. Res.*, *72*, 641–659, doi:10.1175/JAS-D-14-0042.1.

Benedict, J. J., and D. A. Randall (2007), Observed characteristics of the MJO relative to maximum rainfall, *J. Atmos. Sci.*, *64*, 2332–2354.

Ciesielski, P. E., et al. (2014), Quality-controlled upper-air sounding dataset for DYNAMO/CINDY/AMIE: Development and corrections, *J. Atmos. Oceanic Technol.*, *31*, 741–764.

Clayson, C. A., and L. Kantha (2008), On turbulence and mixing in the free atmosphere inferred from high-resolution soundings, *J. Atmos. Oceanic Technol.*, *25*, 833–852.

Davison, J. L. (2014), Investigation of the island effect on mixed layer top and transition layer top elevations using Bragg Scattering Layer (BSL) analysis of clear-air S-Pol radar retrievals at the Gan site during CINDY2011/DYNAMO/AMIE, AMS 31st Conference on Hurricanes and Tropical Meteorology, San Diego, Calif., 4 Jan.

Davison, J. L., R. M. Rauber, and L. Di Girolamo (2013a), A revised conceptual model of the tropical marine boundary layer. Part II: Detecting relative humidity layers using Bragg scattering from S-band radar, *J. Atmos. Sci.*, *70*, 3025–3046.

Davison, J. L., R. M. Rauber, L. Di Girolamo, and M. A. LeMone (2013b), A revised conceptual model of the tropical marine boundary layer. Part III: Bragg scattering layer statistical properties, *J. Atmos. Sci.*, *70*, 3047–3062.

Dewan, E. M. (1981), Turbulent vertical transport due to thin intermittent mixing layers in the stratosphere and other stable fluids, *Science*, *211*, 1041–1042.

Gavrilov, N. M., H. Luce, M. Crochet, F. Dalaudier, and S. Fukao (2005), Turbulence parameter estimations from high-resolution balloon temperature measurements of the MUTSI-2000 campaign, *Ann. Geophys.*, *23*, 2401–2413.

Holloway, C. E., and J. D. Neelin (2009), Moisture vertical structure, column water vapor, and tropical deep convection, *J. Atmos. Sci.*, *66*, 1665–1683.

Hong, S.-Y., and H.-L. Pan (1996), Nonlocal boundary layer vertical diffusion in a medium-range forecast model, *Mon. Weather Rev.*, *124*, 2322–2339.

Kantha, L., and W. Hocking (2011), Dissipation rates of turbulence kinetic energy in the free atmosphere: MST radar and radiosondes, *J. Atmos. Sol. Terr. Phys.*, *73*, 1043–1051.

Kerns, B. W., and S. S. Chen (2014), Equatorial dry air intrusion and related synoptic variability in MJO initiation during DYNAMO, *Mon. Weather Rev.*, *142*, 1326–1343.

Luce, H., T. Mega, M. K. Yamamoto, M. Yamamoto, H. Hashiguchi, S. Fukao, N. Nishi, T. Tajiri, and M. Nakazato (2010), Observations of Kelvin-Helmholtz instability at a cloud base with the middle and upper atmosphere (MU) and weather radars, *J. Geophys. Res.*, *115*, D19116, doi:10.1029/2009JD013519.

Luce, H., R. Wilson, F. Dalaudier, H. Hashiguchi, N. Nishi, Y. Shibagaki, and T. Nakajo (2014), Simultaneous observations of tropospheric turbulence from radiosondes using Thorpe analysis and the VHF MU radar, *Radio Sci.*, *49*, 1106–1123, doi:10.1002/2013RS005355.

Marlton, G. J., R. G. Harrison, K. A. Nicoll, and P. D. Williams (2015), A balloon-borne accelerometer technique for measuring atmospheric turbulence, *Rev. Sci. Instrum.*, *86*, 016109, doi:10.1063/1.4905529.

Ozmidov, R. V. (1965), On the turbulent exchange in a stably stratified ocean, *Atmos. Ocean. Phys.*, *8*, 853–860.

Parsons, D. B., K. Yoneyama, and J.-L. Redelsperger (2000), The evolution of the tropical western Pacific atmosphere-ocean system following the arrival of a dry intrusion, *Q. J. R. Meteorol. Soc.*, *126*, 517–548.

Redelsperger, J.-L., D. B. Parsons, and F. Guichard (2002), Recovery processes and factors limiting cloud-top height following the arrival of a dry intrusion observed during TOGA COARE, *J. Atmos. Sci.*, *59*, 2438–2457.

Thorpe, S. A. (1977), Turbulence and mixing in a Scottish loch, *Philos. Trans. R. Soc. London*, *286A*, 125–181.

Vanneste, J., and P. H. Haynes (2000), Intermittent mixing in strongly stratified fluid as a random walk, *J. Fluid Mech.*, *411*, 165–185.

Williams, P. D., and M. M. Joshi (2013), Intensification of winter transatlantic aviation turbulence in response to climate change, *Nat. Clim. Change*, *3*(7), 644–648.

Wilson, R. (2004), Turbulent diffusivity in the free atmosphere inferred from MST radar measurements: A review, *Ann. Geophys.*, *22*, 3869–3887.

Wilson, R., F. Dalaudier, and F. Bertin (2005), Estimation of the turbulent fraction in the free atmosphere from MST radar measurements, *J. Atmos. Oceanic Technol.*, *22*, 1326–1339.

Wilson, R., H. Luce, F. Dalaudier, and J. Lefrere (2010), Turbulence patch identification in potential density or temperature profiles, *J. Atmos. Oceanic Technol.*, *27*, 977–993.

Wilson, R., F. Dalaudier, and H. Luce (2011), Can one detect small-scale turbulence from standard meteorological radiosondes?, *Atmos. Meas. Tech.*, *4*, 795–804.

Wilson, R., H. Luce, H. Hashiguchi, M. Shiotani, and F. Dalaudier (2013), On the effect of moisture on the detection of tropospheric turbulence from in situ measurements, *Atmos. Meas. Tech.*, *6*, 697–702.

Wilson, R., H. Luce, H. Hashiguchi, N. Nishi, and Y. Yabuki (2014), Energetics of persistent turbulent layers underneath mid-level clouds estimated from concurrent radar and radiosonde data, *J. Atmos. Sol. Terr. Phys.*, *118*, 78–89.

Woodman, R. F., and P. K. Rastogi (1984), Evaluation of effective eddy diffusive coefficients using radar observations of turbulence in the stratosphere, *Geophys. Res. Lett.*, *11*, 243–246.

Yoneyama, K., C. Zhang, and C. N. Long (2013), Tracking pulses of the Madden-Julian oscillation, *Bull. Am. Meteorol. Soc.*, *94*, 1871–1891.

Zhang, J., H. Chen, Z. Li, X. Fan, L. Peng, Y. Yu, and M. Cribb (2010), Analysis of cloud layer structure in Shouxian, China using RS92 radiosonde aided by 95 GHz cloud radar, *J. Geophys. Res.*, *115*, D00K30, doi:10.1029/2010JD014030.